EARTHARXIV PREPRINT REPOSITORY

Preprint Server for Earth Sciences
California Digital Library / Janeway

PEER REVIEW STATUS: This manuscript is a non-peer-reviewed preprint submitted to EarthArXiv.
It is currently undergoing formal peer review at an international scholarly journal. The content may be updated or revised. Please cite this work as a preprint.

Comparative Hydrodynamic Simulation and Field-Based Validation of an Extreme Urban Flood Event in Southern Bali

Golan Geldoffer Mauregar[1,4], Robby Yussac Tallar[1,4,*], Alfrendo Satyanaga[2], Oscar Karnalim[3], James Dwikurnia Sihonggi[4], and Febrian Timotius Sugiarto[4]

[1] Department of Civil Engineering, Universitas Kristen Maranatha, Bandung 40164, Indonesia
[2] School of Engineering and Digital Sciences, Department of Civil and Environmental Engineering, Nazarbayev University, Astana 010000, Kazakhstan
[3] Department of Informatics Engineering, Universitas Kristen Maranatha, Bandung 40164, Indonesia
[4] Center of Excellence (CoE) HydroLink, Universitas Kristen Maranatha, Bandung 40164, Indonesia
*** Correspondence:** robbyyussac@yahoo.com | **Lead Author:** golanlalong98@gmail.com

Abstract

A severe rainstorm on 9–10 September 2025 inundated Denpasar City, Badung Regency, and Gianyar Regency in South Bali, causing 15 fatalities across 188 reported locations. This study simulates the event over 14 sub-catchments (1,146 km²) with HEC-RAS 2D and compares two rainfall inputs: a lumped upstream boundary hydrograph based on Snyder's synthetic unit hydrograph (Method A) and watershed-scale rain-on-grid (Method B). Rainfall came entirely from satellite products, SITHALA for daily totals and PERSIANN-CCS for a 37-hour storm duration, distributed with the Alternating Block Method. The SCS Curve Number method, with a five-class land cover map, Antecedent Moisture Condition I, and an initial abstraction ratio of 0.05, produced 33.1–108.8 mm of effective rainfall (68.6 million m³ of runoff), applied to a 10 × 10 m mesh; depths below 0.20 m were excluded from mapping. Method A flooded 101.92 km² (8.89%), with 50.6% of this area (51.53 km²) deeper than 5 m and hydrograph peaks arriving after the storm window. Method B flooded 80.83 km² (7.05%), of which about 93% was 0.20–2.00 m deep and only 0.39 km² exceeded 5 m. Against 32 field survey points, Method A overestimated depths at its nine inundated points (mean bias +189.8 cm; MAE 249.3 cm) and left 23 points dry. Method B underestimated depths at its six inundated points (bias –74.8 cm; MAE 74.8 cm); for the 26 points it left dry, 81% had an inundated cell within 100 m (median 55.8 m). Rain-on-grid was more suitable for satellite-driven, ungauged applications.

Keywords: flood inundation; HEC-RAS 2D; rain-on-grid method; lumped synthetic hydrograph; Curve Number; field validation; urban hydrology; Bali

Submission Date: November 2026
Subject Category: Hydrology & Water Resources / Natural Hazards
Repository: EarthArXiv (California Digital Library / Janeway)

Funding: BRIN RIIM Wave 10 (Grant No. 57186119503)
License: Creative Commons Attribution 4.0 International (CC BY 4.0)
Data Availability: DEMNAS/SITHALA/PERSIANN-CCS public; models on request

Research Article

Comparative Hydrodynamic Simulation and Field-Based Validation of an Extreme Urban Flood Event in Southern Bali

Golan Geldoffer Mauregar[1], Robby Yussac Tallar[1,*], Alfrendo Satyanaga[2], Oscar Karnalim[3], James Dwikurnia Sihonggi[4], and Febrian Timotius Sugiarto[4]

[1] Civil Engineering Department, Universitas Kristen Maranatha, Jln. Prof. drg. Surya Sumantri No. 65, Bandung 40164, Indonesia

[2] School of Engineering, Department of Civil and Environmental Engineering, Nazarbayev University, Astana 010000, Kazakhstan

[3] Informatics Engineering Department, Universitas Kristen Maranatha, Bandung 40164, Indonesia

[4] Center of Excellence (CoE) HydroLink, Universitas Kristen Maranatha, Bandung 40164, Indonesia

* Correspondence: robbyyussac@yahoo.com; Tel.: +62-813-2133-0032

Abstract

A severe rainstorm on 9–10 September 2025 inundated Denpasar City, Badung Regency, and Gianyar Regency in South Bali, causing 15 fatalities across 188 reported locations. This study simulates the event over 14 sub-catchments (1,146 km²) with HEC-RAS 2D and compares two rainfall inputs: a lumped upstream boundary hydrograph based on Snyder's synthetic unit hydrograph (Method A) and watershed-scale rain-on-grid (Method B). Rainfall came entirely from satellite products, SITHALA for daily totals and PERSIANN-CCS for a 37-hour storm duration, distributed with the Alternating Block Method. The SCS Curve Number method, with a five-class land cover map, Antecedent Moisture Condition I, and an initial abstraction ratio of 0.05, produced 33.1–108.8 mm of effective rainfall (68.6 million m³ of runoff), applied to a 10 × 10 m mesh; depths below 0.20 m were excluded from mapping. Method A flooded 101.92 km² (8.89%), with 50.6% of this area (51.53 km²) deeper than 5 m and hydrograph peaks arriving after the storm window. Method B flooded 80.83 km² (7.05%), of which about 93% was 0.20–2.00 m deep and only 0.39 km² exceeded 5 m. Against 32 field survey points, Method A overestimated depths at its nine inundated points (mean bias +189.8 cm; MAE 249.3 cm) and left 23 points dry. Method B underestimated depths at its six inundated points (bias −74.8 cm; MAE 74.8 cm); for the 26 points it left dry, 81% had an inundated cell within 100 m (median 55.8 m). Rain-on-grid was more suitable for satellite-driven, ungauged applications.

Keywords: *flood inundation; HEC-RAS 2D; rain-on-grid method; lumped synthetic hydrograph; Curve Number; field validation*

1. Introduction

Heavy rainfall triggers flooding, and land-use alterations systematically transform these triggers into disasters (Lestari & Herdiansyah, 2024). Over the past decade, Bali has recorded a marked increase in flood intensity (Badan Meteorologi, Klimatologi, dan Geofisika [BMKG], 2024). Setiawan (2012) reported a shift in the island's climate type from relatively wet toward somewhat drier conditions, together with changes in the monthly rainfall distribution. Changing and potentially more intense precipitation in Bali may increase the probability of extreme flooding. Concurrently, rapid urban expansion continues to strip away natural infiltration surfaces, severely constraining drainage capacities.

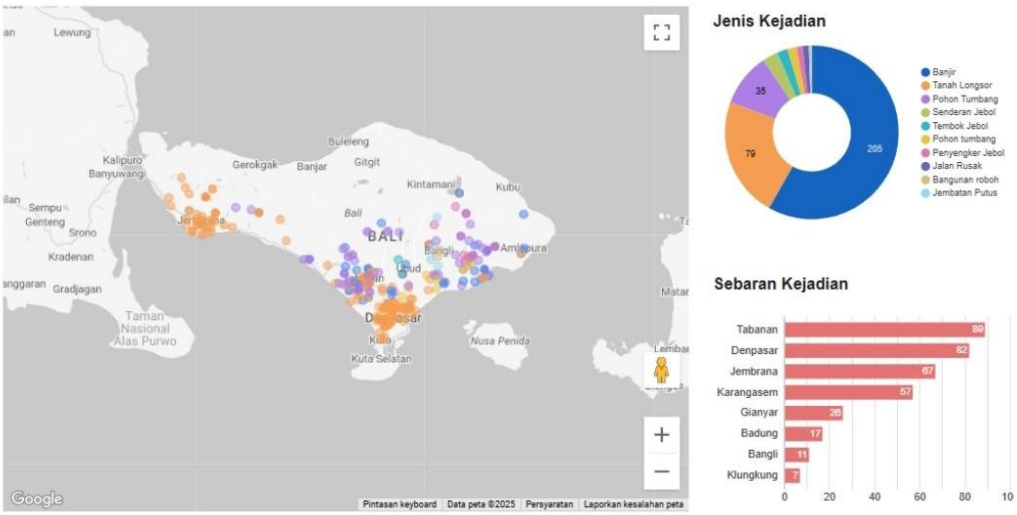


Figure 1. Flood-prone areas and the distribution of disaster events in Bali Province in 2025 (BPBD Provinsi Bali, 2025).

Through 2024, BMKG documented numerous recurring flood hotspots—such as Jalan Pura Demak, Jalan Bumi Ayu, and Jalan Raya Puputan–Moh. Yamin—where inundation severely disrupts the tourism sector, the backbone of the regional economy (Sutrisnawati, 2018). This pattern escalated dramatically in September 2025. The Regional Disaster Management Agency (BPBD Provinsi Bali, 2025) mapped flood events on 10 September 2025, revealing that disasters struck 89 locations in Gianyar Regency, 82 in Denpasar City, and 17 in Badung Regency out of 356 total provincial disaster incidents, 205 of which were floods (Figure 1). Denpasar experienced the highest fatality rate with 11 deaths. The vast geographic spread and substantial loss of life cement this event as the most severe flood disaster documented in the province.

Previous flood studies in Bali have generally stopped short of simulating physics-based, validated inundation depths for actual events. Kusmiyarti et al. (2018) mapped flood risk in Denpasar using a weighted overlay of hazard indicators, lacking both a hydrograph and a hydrodynamic process-based depth output. Adnyana and Wiguna (2025) applied the Topographic Wetness Index (TWI) in the Yeh Ho Watershed as a rapid assessment tool. Prabandari et al. (2025) derived the design flood discharge for the Palasari Dam using the SCS Curve Number in HEC-HMS, but their analysis concluded at reservoir inflows rather than urban inundation mapping. Two recent 2026 studies initiated the transition toward physical simulation. Habibi and Nisa (2026) applied HEC-RAS to the same 9–10 September 2025 event but restricted their domain to a single watershed (Tukad Badung) and validated their mapping using a binary hit rate—a pattern-matching metric that can falsely credit a model for overestimating flood extent without verifying water depth accuracy (Stephens et al., 2014). Meanwhile, Pranoto et al. (2026) coupled HEC-HMS and HEC-RAS 2D for the Cimanceuri River Basin in Java and compared simulated inundation patterns with aerial imagery rather than with surveyed depths.

A two-dimensional (2D) hydrodynamic model can receive precipitation inputs via two primary mechanisms: as a lumped discharge hydrograph injected at the domain boundary, or as direct rainfall applied across the computational mesh (rain-on-grid). In ungauged catchments, the boundary hydrograph approach relies heavily on synthetic parameters (e.g., Kirpich's time of concentration and Snyder's basin lag coefficient) that are highly susceptible to bias since they cannot be calibrated against streamflow records. Injecting a synthetic hydrograph at the upstream end of the main channel may also (1) force the entire effective runoff volume into a single-intake path, limiting the inundation of lateral urban drainage networks; (2) concentrate flow in steep, narrow valleys and cause channel

bottlenecking; and (3) introduce a double-lagging effect, as the overland flow travel time calculated by the 2D routing is added to the lag time already inherent in Snyder's formula, which may shift the peak discharge out of the actual storm window. In contrast, the rain-on-grid method applies rainfall to every computational cell, so that all tributaries fill simultaneously, although it requires a shallow-depth threshold (e.g., 0.20 m) to remove superficial sheet-flow noise. This study examines these expected differences against field observations.

This study bridges these methodological gaps by linking satellite-derived design rainfall, land-cover-based runoff parameterization, and 2D comparative hydrodynamic simulation (lumped boundary hydrograph vs. rain-on-grid) combined with a 0.20 m noise threshold. We expand the modeling domain to 14 sub-catchments across three regencies and rigorously validate the outputs against 32 post-disaster field survey points, distinctly separating exact-cell depth comparisons from spatial tolerance buffers (neighborhood verification) as proposed by Ebert (2008).

2. Materials and Methods

2.1. Study Area and Dataset Compilation

Denpasar City, Badung Regency, and Gianyar Regency form a contiguous corridor in southern Bali that conveys rainfall from the island's interior to the southern coast (Figures 2 and 3). Three primary rivers—the Ayung, Badung, and Mati Rivers—traverse this urban corridor, converging at Denpasar located at their downstream outlets (Kusmiyarti et al., 2018). Over half of the study area features elevations ranging from −4 m to 250 m above sea level, encompassing highly flat urban cores. This mild gradient significantly retards natural drainage, allowing floodwaters to pool across streets and low-lying residential blocks. Conversely, the northern terrain ascends steeply to 2,090 m near Mount Agung.

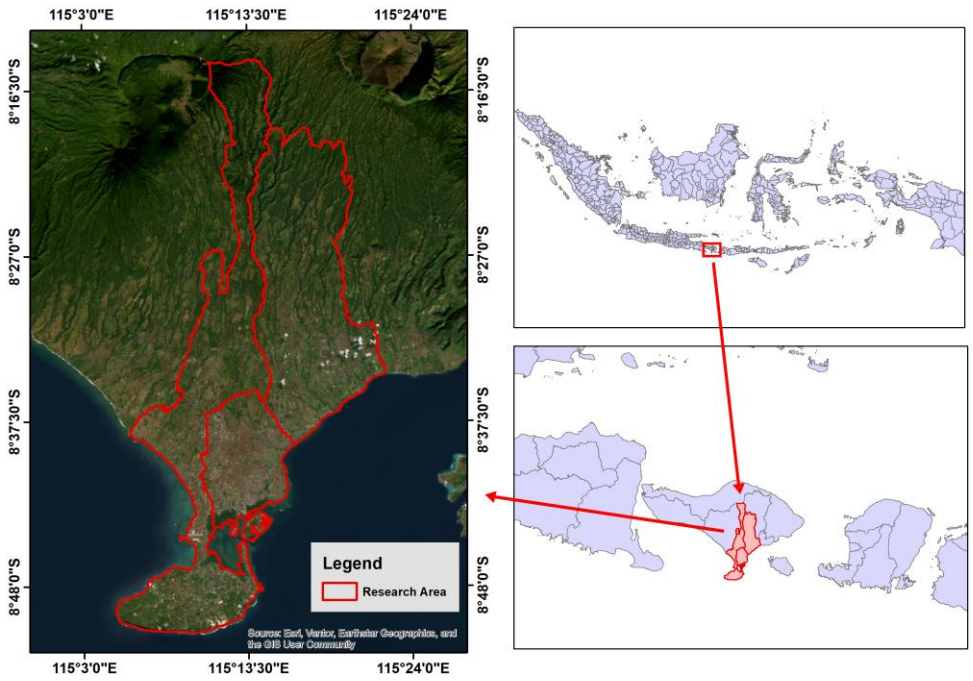


Figure 2. Map of the study area encompassing the Denpasar, Badung, and Gianyar corridor in South Bali.

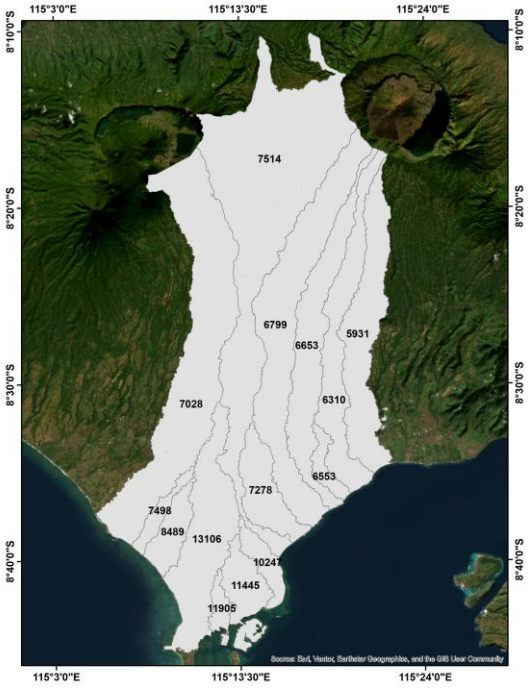


Figure 3. The 14 sub-catchments (labelled by catchment ID) delineated within the study area.

This research relies on four primary spatial databases: topography, land cover, precipitation, and soil physical properties. The resolution, sources, and functional utility of each dataset are comprehensively summarized in Table 1. Elevation data were obtained from DEMNAS (Badan Informasi Geospasial [BIG], n.d.) and daily rainfall from SITHALA (Balai Hidrologi dan Lingkungan Keairan [BHLK], 2025).

Table 1. Summary of spatial and hydrometeorological datasets utilized for model inputs.

Dataset	Data Source	Resolution / Scale	Modeling Function
Topography (DEM)	DEMNAS (Distributed via Ina-Geoportal, BIG)	0.27 arcsec (~8.3 m); Vertical datum EGM2008	Base terrain for the 10 × 10 m HEC-RAS 2D computational mesh and sub-catchment delineation.
Precipitation	SITHALA Satellite (Bias-corrected GPM-IMERG) & PERSIANN-CCS	Daily (SITHALA) & Hourly (PERSIANN)	R24 for Mononobe-ABM distribution and the 37-hour continuous storm duration tracking.
Land Cover	Sentinel-2 SR Harmonized imagery (Google Earth Engine, 2025)	10 m; 5 land cover classes	Determination of the runoff Curve Number (CN) and Manning's roughness coefficients (n).
Hydrologic Soil Group	HYSOGs250m (Ross et al., 2018)	250 m	Determination of potential retention (S) and initial abstraction (Ia) based on soil type (Group D).

2.2. Methodological Framework

This study integrates the four spatial and hydrological datasets into a unified processing pipeline. The data were processed using geographic information systems (ArcGIS), cloud-based remote sensing (Google Earth Engine), and parametric mathematical modeling (Microsoft Excel) to generate the flood design inputs. These inputs were comparatively executed in HEC-RAS 2D under two distinct schemes: Method A (injection of a synthetic unit hydrograph at the upstream boundary) and Method B (direct effective rainfall precipitation on the computational mesh / rain-on-grid). Both hydrodynamic simulation outputs were subsequently filtered to eliminate sheet-flow depth noise

below 0.20 m, before ultimately undergoing statistical performance validation against 32 field survey data points. The overall methodology is illustrated in Figure 4.

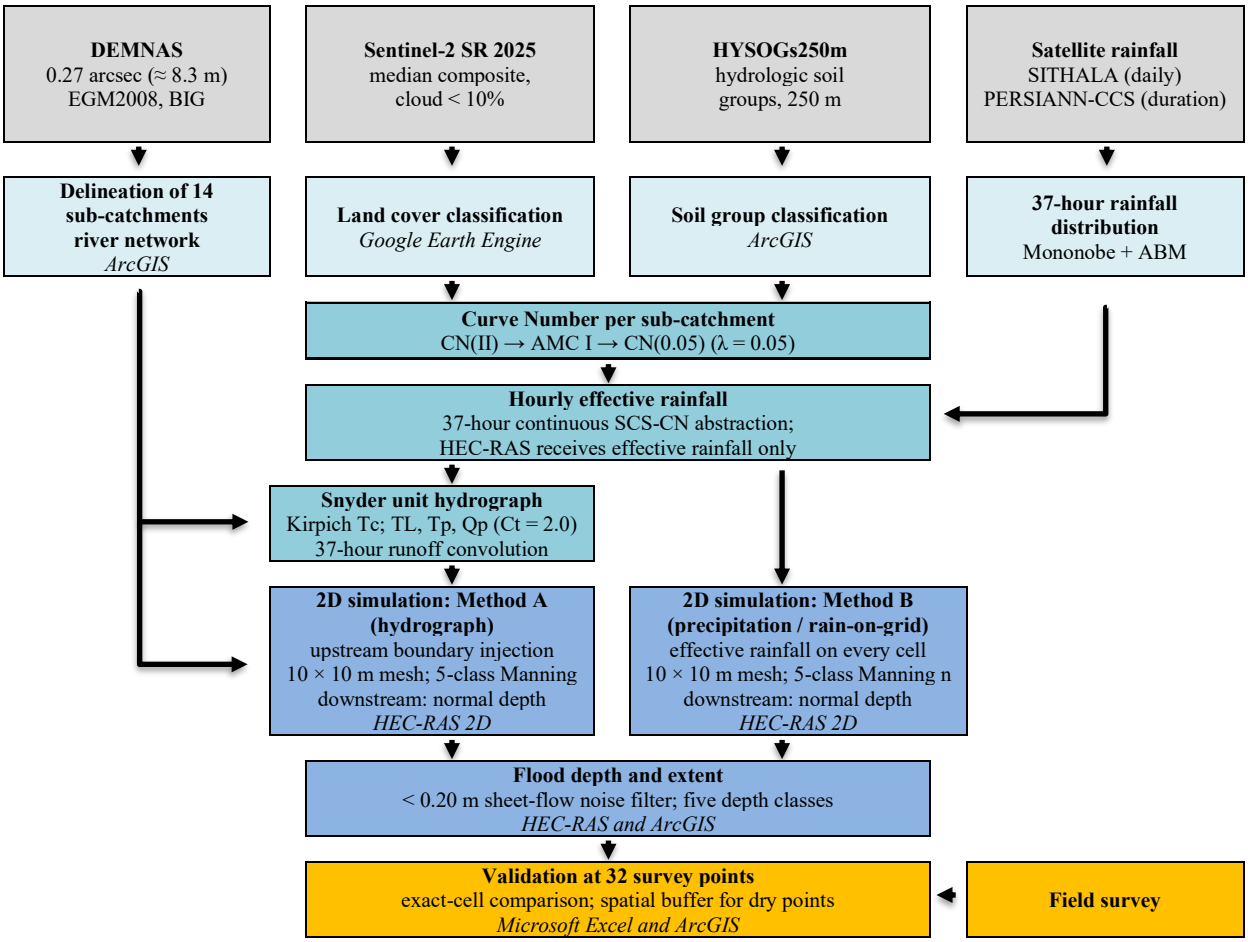


Figure 4. Flowchart of the comparative hydrodynamic flood modeling methodology.

2.3. Land Cover Classification and Hydrological Parameterization

Land cover classification was derived from a 2025 median composite of Sentinel-2 Surface Reflectance (SR) imagery with cloud cover below 10%, processed using Google Earth Engine. A Random Forest algorithm classified the study area strictly into five classes: forest, grassland, bare land, built-up area, and water body. The distinction between grassland (good condition, >75% cover) and bare land (poor condition/bare soil, <50% cover) was rigorously maintained because they generate significantly different runoff responses and surface roughness coefficients.

Hydrological parameterization was founded on the SCS Curve Number (CN) method. Hydrologic Soil Group data were extracted from the HYSOGs250m global raster (Ross et al., 2018), revealing that Group D (soils with very slow infiltration rates) dominated all 14 sub-catchments. Because the event occurred in the 2025 dry season (BMKG, 2025) and the cumulative 5-day antecedent rainfall derived from PERSIANN-CCS (4–8 September 2025) ranged only from 1.09 to 7.10 mm, all sub-catchments were classified under Antecedent Moisture Condition I (AMC I). The standard AMC II curve numbers were converted to AMC I using Equation (1).

$$(1) \quad CN_{\mathrm{I}} = (4.2 \times CN_{\mathrm{II}}) \,/\, (10 - 0.058 \times CN_{\mathrm{II}})$$

Furthermore, Hawkins et al. (2002) demonstrated that the conventional initial abstraction ratio (0.20) is frequently inaccurate and proposed a 0.05 ratio. Consequently, the CN values were adjusted to a 0.05 basis utilizing Equation (2). The maximum potential retention (S) and initial abstraction (Ia) were subsequently calculated via Equations (3) and (4).

$$(2) \quad CN_{0.05} = 100 \,/\, [1.879 \times ((100 \,/\, CN_{\mathrm{I}}) - 1)^{1.15} + 1]$$

$$(3) \quad S = (25400 \,/\, CN_{0.05}) - 254$$

$$(4) \quad I_{\mathrm{a}} = 0.05 \times S$$

Manning's roughness coefficients (n) for each land cover class were assigned following standard hydraulic values from Chow (1959) and the National Land Cover Database (NLCD) classification. The areal proportions, flow roughness coefficients, and converted hydrological parameters for the five land cover classes are comprehensively summarized in Table 2.

Table 2. Hydrological and hydrodynamic parameterization based on five land cover classes for Hydrologic Soil Group (HSG) D (Manning's n adapted from Chow, 1959).

Land Cover Class	Areal Proportion (%)	Initial Curve Number (AMC II, λ=0.20)	Final Curve Number (AMC I, λ=0.05)	Manning's Roughness (n)
Forest	31.88%	77	42.2	0.360
Built-up Area	26.66%	92	75.9	0.068
Bare Land (Poor Condition)	20.46%	89	68.6	0.0368
Grassland (Good Condition)	20.46%	80	48.3	0.100
Water Body	0.54%	100	100.0	0.030

2.4. Design Rainfall Analysis

The design rainfall encompasses a 37-hour continuous storm duration (tracked via PERSIANN-CCS), divided into two segments: 19 hours on 9 September and 18 hours on 10 September 2025. The maximum daily rainfall (R24) for each calendar day was extracted from the bias-corrected SITHALA satellite dataset. Hourly rainfall intensities were derived using the Mononobe equation (Equation 5), and the incremental hourly blocks were temporally arranged using the Alternating Block Method (ABM).

$$(5) \quad I_{\mathrm{t}} = (R_{24} \,/\, 24) \times (24 \,/\, t)^{2/3}$$

Because the duration of each segment is less than 24 hours, summing the incremental blocks from the pure Mononobe equation would fail to reach 100% of the total daily R24. Consequently, a proportional normalization was applied to the ABM blocks using Equations (6) and (7) to ensure that the total volume of the 19-hour and 18-hour segments perfectly matched the recorded satellite daily rainfall.

$$(6) \quad p_{\mathrm{t}} = \Delta p_{\mathrm{ABM,t}} \,/\, \Sigma \Delta p_{\mathrm{t}}$$

$$(7) \quad P_{\mathrm{t}} = p_{\mathrm{t}} \times R_{24}$$

The effective rainfall was subsequently computed utilizing continuous SCS-CN abstraction across the 37-hour window without resetting the cumulative totals at the midnight boundary (Equation 8). This continuous accounting ensures that the progressive soil saturation effect is accurately modeled.

$$(8) \quad \Sigma P_{\mathrm{eff}}(\mathrm{t}) = [\Sigma P(\mathrm{t}) - I_{\mathrm{a}}]^2 \,/\, [\Sigma P(\mathrm{t}) - I_{\mathrm{a}} + S]$$

2.5. Design Flood Hydrograph Derivation (Method A)

As the primary comparative baseline, the design flood hydrograph was derived by convolving the 37-hour effective rainfall with Snyder's synthetic unit hydrograph (Snyder, 1938). The time of concentration (Tc) was calculated based on Kirpich's formula (Kirpich, 1940). The lag time (TL), time to peak (Tp), and peak discharge per unit of effective rainfall (Qp) were formulated in Equations (9) through (11). Ct is the basin coefficient; based on extensive empirical calibration by Bedient and Huber (1992), which observed Ct values ranging from 1.8 to 2.2 across various basins, this study adopted the recommended median value of 2.0. L is the main channel length, Lc is the distance from the basin centroid to the outlet, Tr is the unit rainfall duration, and A is the sub-catchment area.

$$T_{\mathrm{L}} = C_{\mathrm{t}} \left(L \times L_{\mathrm{c}}\right)^{0.3} \quad (9)$$

$$T_{\mathrm{p}} = T_{\mathrm{L}} + \left(T_{\mathrm{r}} / 2\right) \quad (10)$$

$$Q_{\mathrm{p}} = \left(2.75 \times A\right) / T_{\mathrm{p}} \quad (11)$$

2.6. Comparative 2D Hydrodynamic Modeling

The unsteady flow simulation solved the two-dimensional Saint-Venant equations (Continuity and Momentum) using HEC-RAS 2D (U.S. Army Corps of Engineers, Hydrologic Engineering Center, 2016). The computational mesh was established at a fixed 10 × 10 m resolution derived from DEMNAS data. Surface roughness parameters were strictly defined based on the 5 land cover classes in Table 2. To ensure an equitable inter-method comparison, the downstream boundary condition for both methods was set using a Normal Depth assumption calculated from the respective main channel bed slopes, and the simulations were executed for an identical 37-hour duration. This comparative testing was conducted under two distinct schemes:

• Method A (Lumped Boundary Hydrograph): The convolved hydrograph for each sub-catchment (Snyder's output) was entirely injected at the highest upstream node of the main channel, allowing the water to route downstream across the mesh.

• Method B (Rain-on-Grid): The continuous 37-hour effective rainfall time series was applied directly as a precipitation source term onto every 10 × 10 m cell across the computational domain.

2.7. Depth Thresholding and Field Validation Procedure

In watershed-scale modeling—particularly within the rain-on-grid method—the direct application of rainfall inherently generates a superficial layer of overland flow (sheet flow) that blankets the topography prior to channel concentration. To prevent this shallow noise from artificially inflating the flood inundation area, a strict depth threshold of 0.20 meters was applied during post-processing. All pixels with a maximum simulated depth below 20 cm were completely excluded from the flood hazard mapping in both methods.

The maximum simulated depths were subsequently validated against 32 post-disaster field survey points measured in July 2026. The field survey depths represent unaltered, original post-disaster measurements. For the hydrodynamic simulation outputs (Methods A and B), flood depths below 0.20 m were excluded to eliminate shallow sheet-flow noise in regional flood mapping. The validation procedure bifurcated the evaluation: (1) exact-cell comparison, reporting the Mean Absolute Error (MAE) and bias for points where the exact coordinates were simulated as inundated; and (2) spatial buffer search (neighborhood verification), specifically designed for survey points falling on dry cells. For dry points, the search expanded radially from the survey coordinates to locate the nearest inundated cell presenting a similar depth, effectively quantifying spatial shift tolerances induced by the averaging of microtopographic resolution in the DEM. Simulated depths at the survey points were evaluated directly against field measurements to preserve point-scale error statistics.

3. Results

3.1. Hydrological Parameters and Effective Runoff Volumes

Across the total study area of 1,146.2 km², the HYSOGs250m classification confirmed that all 14 sub-catchments were heavily dominated by Hydrologic Soil Group (HSG) D, characterized by very slow infiltration capacities. The calculated Curve Number (CN) parameters, adjusted for dry antecedent moisture conditions (AMC I) and a 0.05 initial abstraction ratio, yielded composite CN0.05 values ranging from 51.7 (Sub-catchment 7514, containing the highest forest cover at 49.9%) to 72.0 (Sub-catchment 10247, dominated by 77.2% built-up area). The maximum potential retention (S) was recorded between 98.8 mm and 237.7 mm.

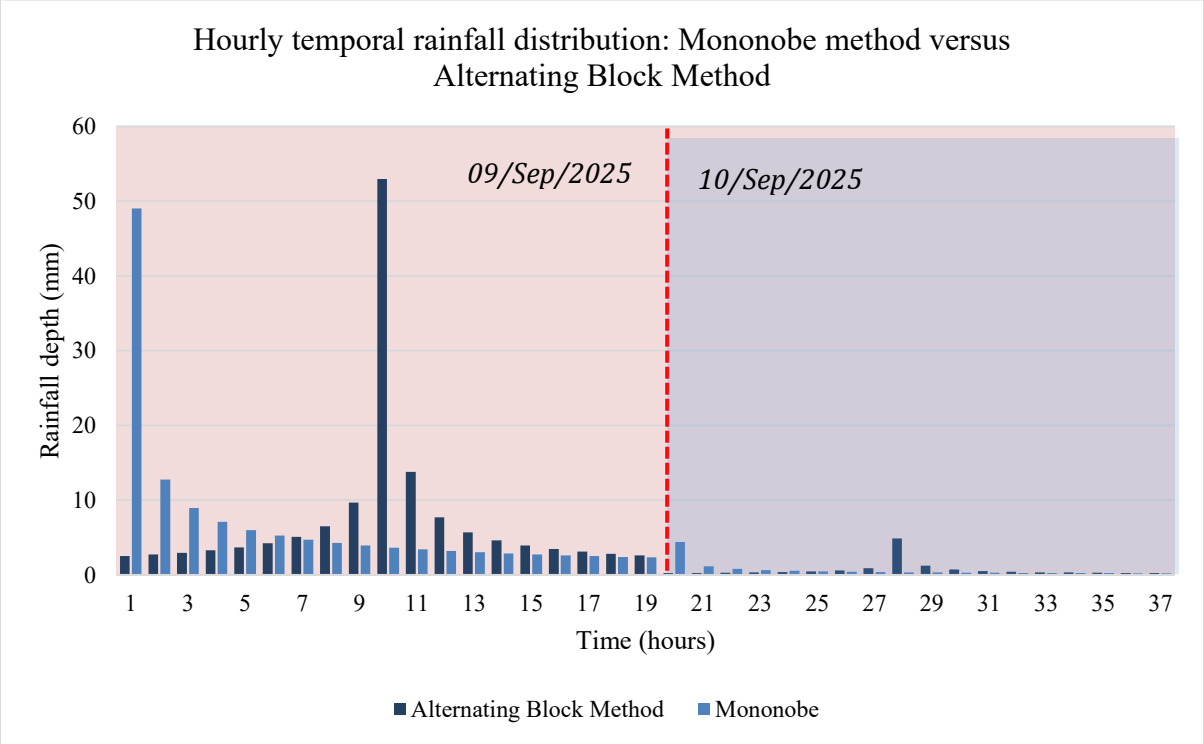


Figure 5. Hourly rainfall distribution (Chronological Mononobe vs. Alternating Block Method) on the representative Sub-catchment 7028.

The runoff abstraction utilizing the 37-hour Mononobe-ABM distribution demonstrated that from the actual varying rainfall across the sub-catchments, the cumulative volume of effective rainfall successfully converted into surface runoff reached 68.64 million m³ across the entire study area. If the

region had been under normal soil moisture conditions (AMC II) prior to the storm, mathematical sensitivity testing indicates that the effective runoff volume would have surged drastically by 33% to 95%, reaching 111.22 million m³, with runoff coefficients sharply increasing from the 0.28–0.62 range up to 0.55–0.82.

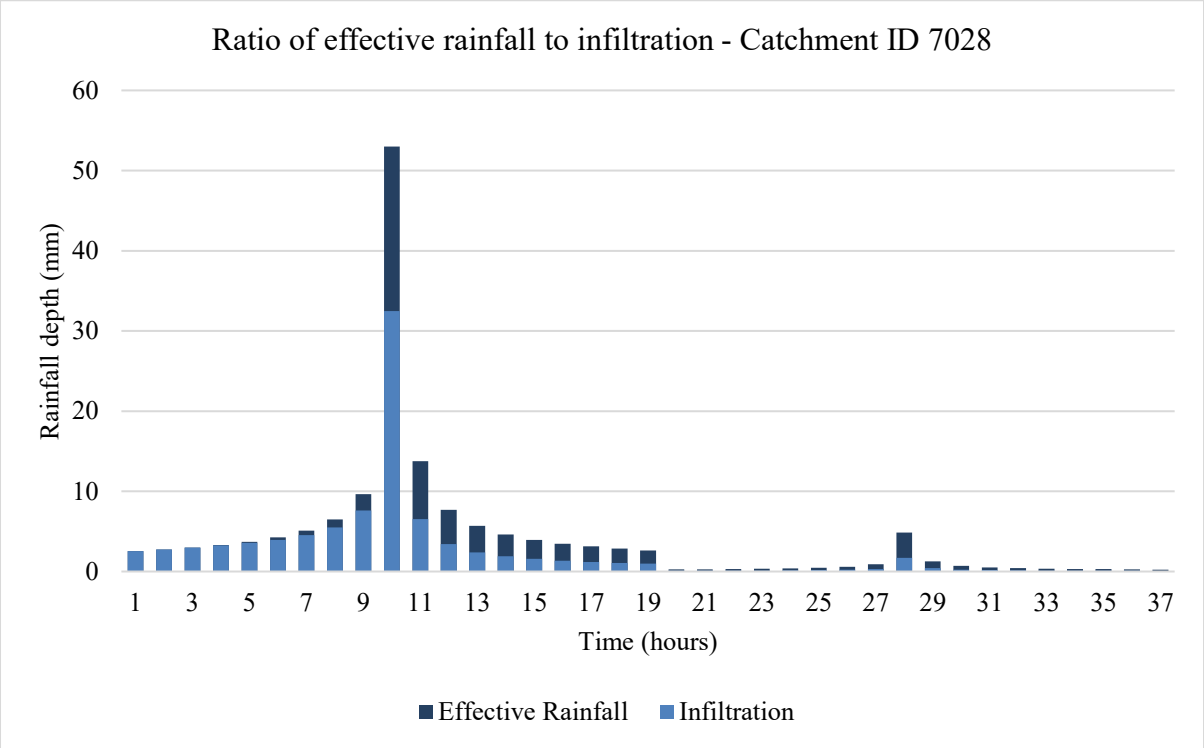


Figure 6. The proportion of effective rainfall (runoff) versus infiltration capacity in Sub-catchment 7028 based on AMC I conditions.

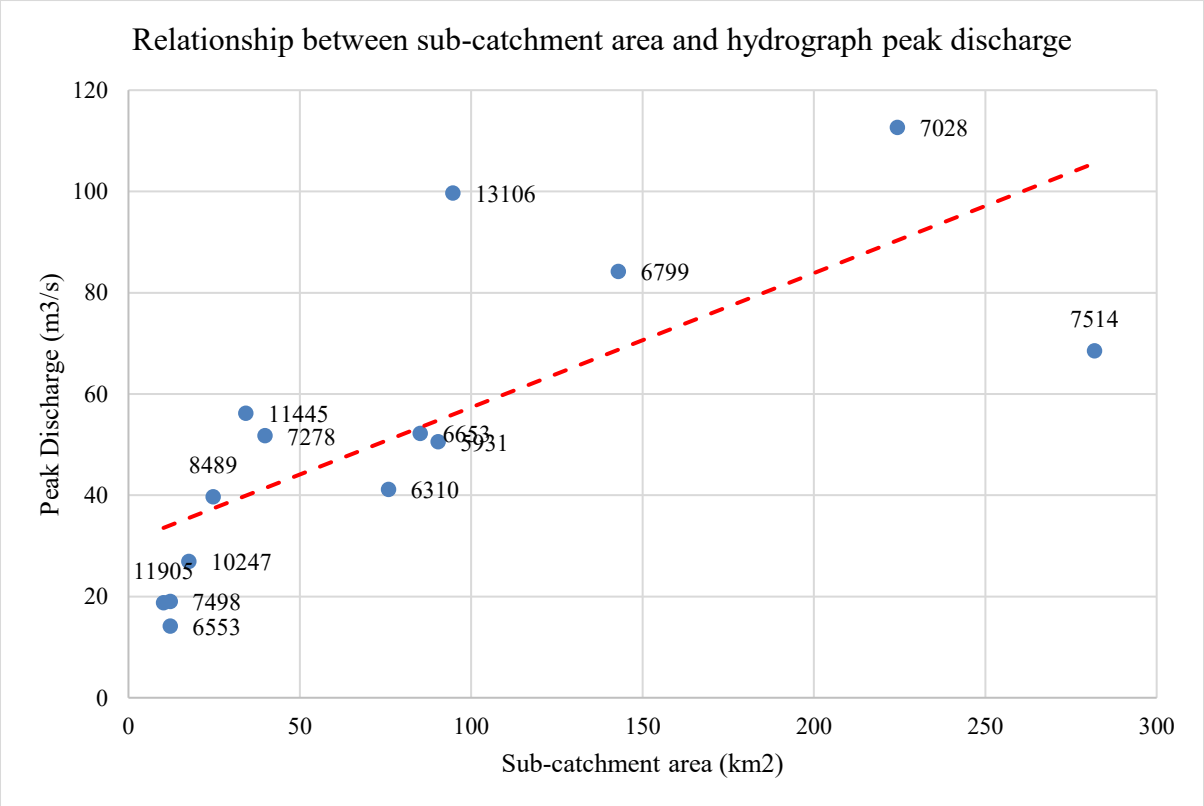


Figure 7. Relationship between sub-catchment area and the design hydrograph peak discharge (Method A).

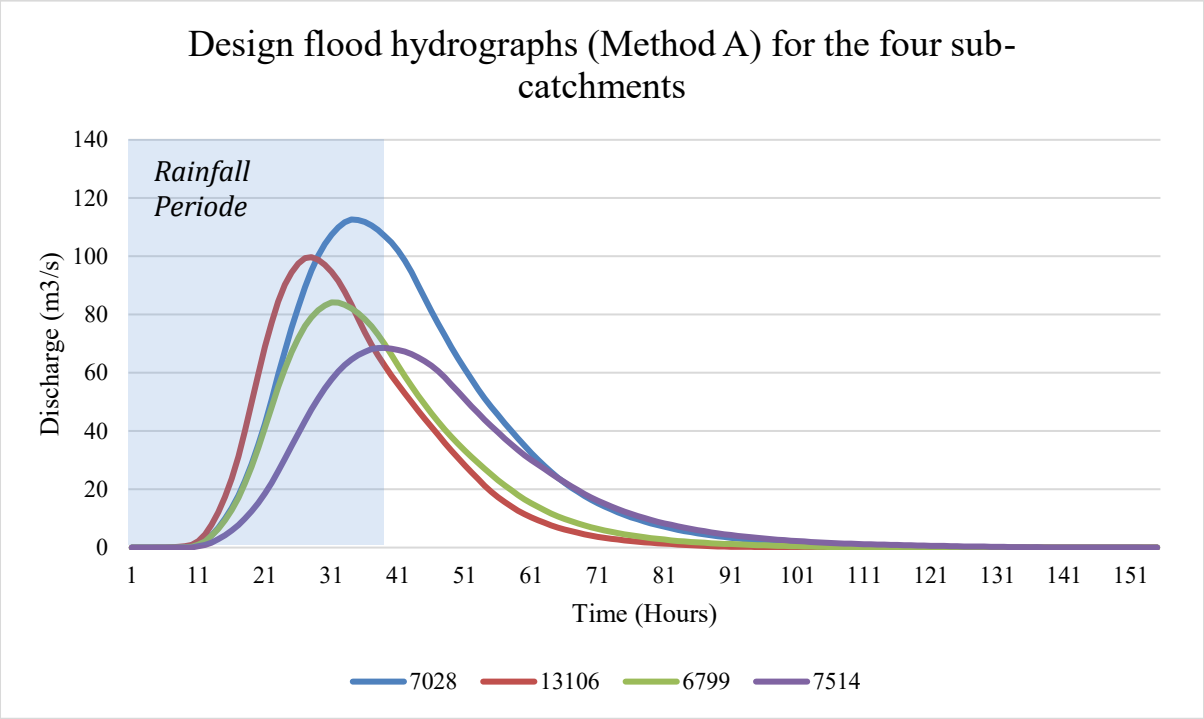


Figure 8. Design flood hydrograph curves (Method A) for the top 4 sub-catchments. The time to peak significantly exceeds the 37-hour rainfall duration.

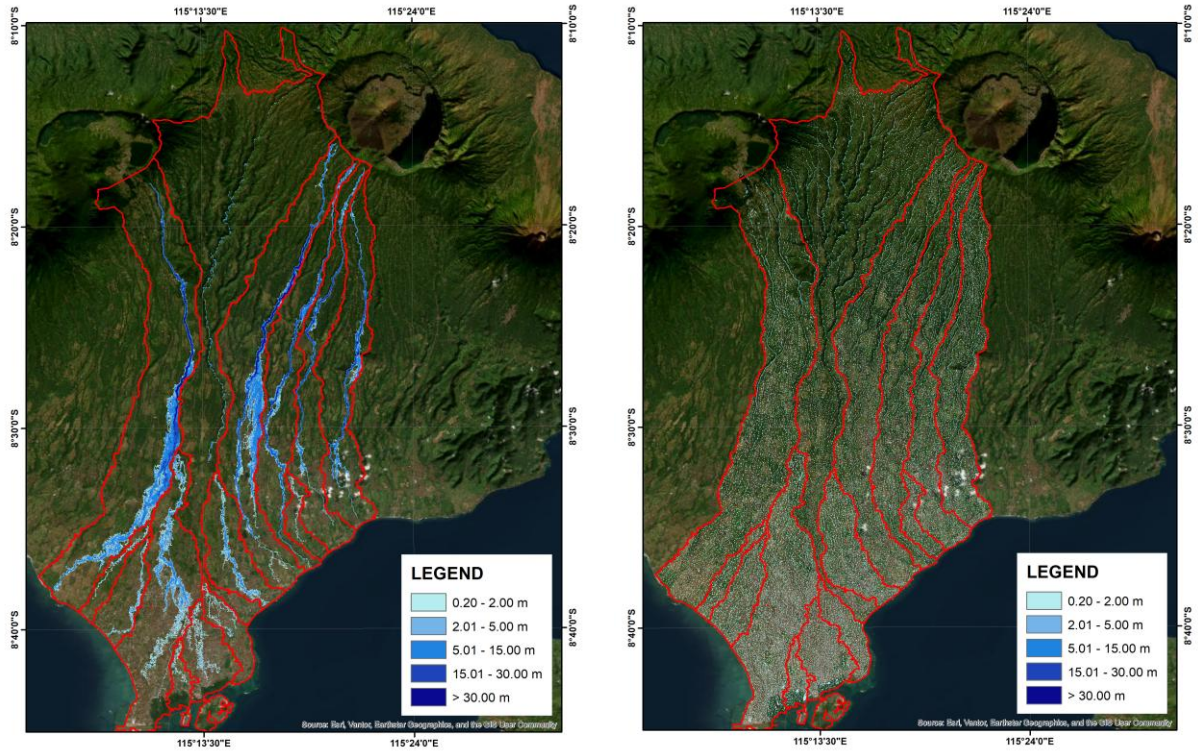
3.2. Comparative Hydrodynamic Inundation: Lumped Boundary Hydrograph vs. Rain-on-Grid

Applying the 0.20 m depth threshold to filter sheet-flow noise revealed marked differences between Method A (hydrograph injection) and Method B (rain-on-grid). Both methods were derived from the same effective runoff depth (68.64 million m³ in total), although the Method A hydrographs extend beyond the 37-hour simulation window (see below). The spatial distribution of the inundated areas is compared in Table 3 and illustrated in Figure 9.

Table 3. Inundated area per sub-catchment and depth class for Method A (lumped boundary hydrograph) and Method B (rain-on-grid), after excluding depths below 0.20 m.

Catchment ID	Class I: 0.20 - 2.00 m		Class II: 2.01 - 5.00 m		Class III: 5.01 - 15.00 m		Class IV: 15.01 - 30.00 m		Class V: > 30.00 m		Total per catchment	
	A (km²)	B (km²)	A (km²)	B (km²)	A (km²)	B (km²)	A (km²)	B (km²)	A (km²)	B (km²)	A (km²)	B (km²)
10247	1.22	2.13	0.42	0.04	0.05	0.00	0.00	0.00	0.00	0.00	1.69	2.18
11445	2.26	3.65	0.76	0.02	0.03	0.00	0.00	0.00	0.00	0.00	3.06	3.68
11905	0.56	1.42	0.23	0.01	0.00	0.00	0.00	0.00	0.00	0.00	0.79	1.43
13106	5.64	11.73	5.71	0.64	3.05	0.00	0.01	0.00	0.00	0.00	14.41	12.37
5931	0.99	6.55	1.55	0.44	3.24	0.01	1.75	0.00	0.21	0.00	7.75	7.00
6310	1.03	5.51	1.35	0.35	2.42	0.02	1.69	0.00	0.21	0.00	6.70	5.88
6553	0.54	1.12	0.22	0.03	0.02	0.00	0.00	0.00	0.00	0.00	0.77	1.15
6653	1.31	5.10	1.92	0.47	3.89	0.03	2.28	0.00	0.30	0.00	9.69	5.60
6799	3.17	8.69	4.44	0.52	9.62	0.01	3.23	0.00	1.56	0.00	22.02	9.23
7028	3.16	12.18	5.94	0.97	10.94	0.13	3.74	0.00	1.32	0.00	25.09	13.28

7278	1.85	4.78	1.89	0.22	1.04	0.00	0.00	0.00	0.00	0.00	4.78	4.99
7498	0.69	1.33	0.35	0.06	0.04	0.00	0.00	0.00	0.00	0.00	1.08	1.39
7514	0.70	8.39	0.60	1.09	0.66	0.17	0.07	0.00	0.00	0.00	2.02	9.66
8489	0.96	2.80	0.93	0.20	0.17	0.00	0.00	0.00	0.00	0.00	2.06	3.00
Total per class	24.08	75.37	26.31	5.07	35.16	0.39	12.78	0.00	3.59	0.00	-	-



(a) **(b)**

Figure 9. Spatial distribution of simulated maximum flood depths (depths below 0.20 m excluded): (a) Method A (lumped boundary hydrograph); (b) Method B (rain-on-grid).

Based on Table 3, Method A (Hydrograph) cumulatively inundated 101.92 km² (8.89% of the study area). However, this configuration produced physically questionable depths. Forcing the entire flood volume through a single upstream injection point is associated with severe channel bottlenecking, and over half (50.56%) of the Method A inundated area (51.53 km²) was concentrated at depths exceeding 5 m, of which 16.37 km² was at depths of 15 m to beyond 30 m. Spatial analysis shows that these depths are almost entirely located in five of the steepest sub-catchments (7028, 6799, 6653, 5931, and 6310), consistent with water stacking vertically inside narrow channels rather than dispersing laterally into urban floodplains, as seen in Figure 9a, where the inundation is deeply constrained within the upstream reaches. No survey point lies inside these incised channels, so these depths could not be checked directly; the overestimation at Points 11, 12, and 32 (Section 3.3) is the available point-based evidence.

Beyond the depth anomalies, Method A also showed a double-lagging effect. The convolution of Snyder's synthetic unit hydrograph shifted the time to peak (tp) to hours 16 through 38 from the start of the rainfall, with the base flow duration (Tb) extending between 61 and 151 hours. Because this hydrograph is re-injected at the upstream nodes of the 2D mesh, the peak wave must additionally travel an overland flow distance of 11.7 to 76.9 km, causing the peak discharge to arrive at Denpasar City long after the actual 37-hour storm window (10 September 2025) had concluded.

Method B (Rain-on-Grid) did not show either of these artifacts. By distributing the precipitation across all 10 × 10 m cells, the inundation responded to the topographic morphology more organically, as seen in Figure 9b. The total flooded area was 80.83 km² (7.05% of the study area) after applying the 0.20 m threshold, which removed 58.0% of the unfiltered rain-on-grid wet area (192.4 km²). The area deeper than 5 m was reduced by a factor of more than 130 relative to Method A, to 0.39 km² (0.48% of the total flooded area), and depths greater than 15 m did not occur. Method B also inundated lateral urban depressions and tributary networks that the single-intake hydrograph model did not reach.

3.3. Field Validation Results and Spatial Tolerance Analysis

The different ways in which the two methods distribute water affected their agreement with the 32 post-disaster field survey points (Figure 10).

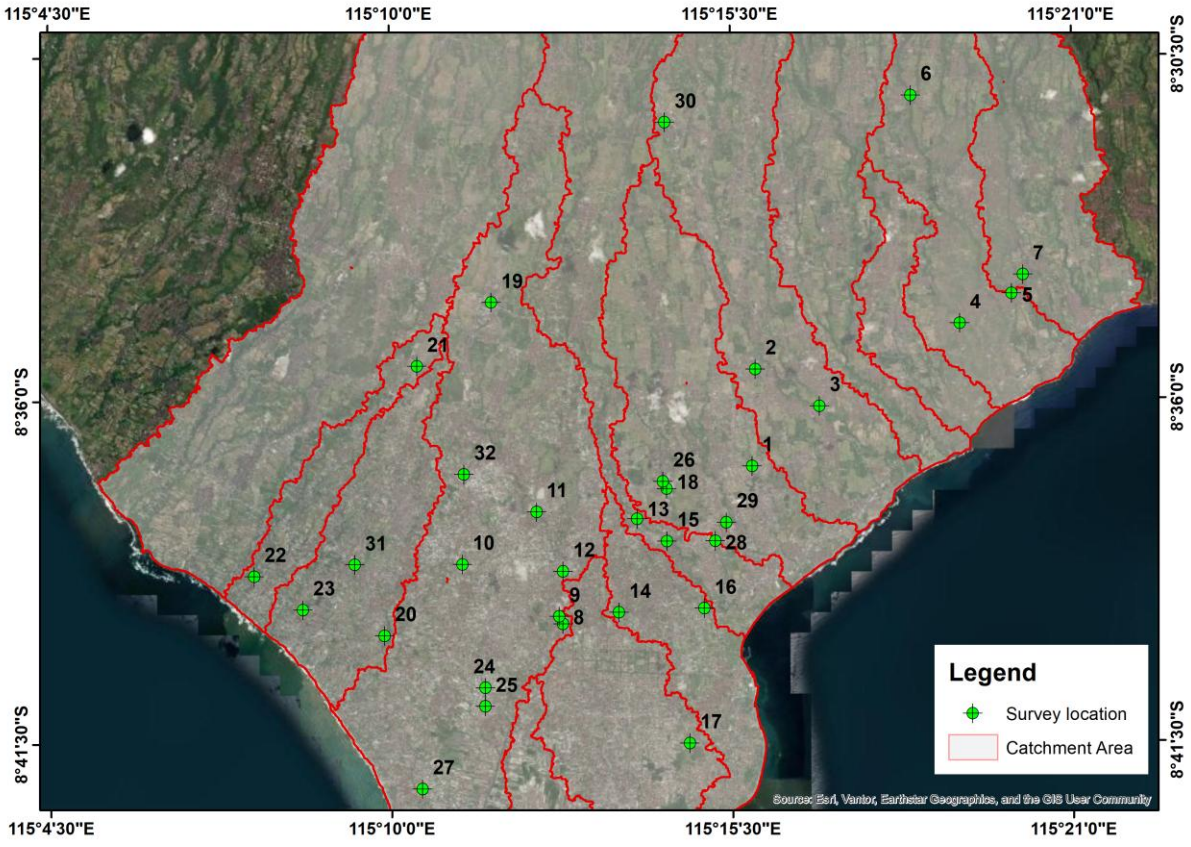


Figure 10. Locations of the 32 post-disaster field survey points (numbered) relative to the sub-catchment boundaries.

Table 4 lists the 13 survey points at which at least one method simulated inundation at the exact cell (nine points for Method A and six for Method B; Points 27 and 32 are inundated in both).

Table 4. Surveyed versus simulated maximum depths at the survey points inundated at the exact cell by at least one method (n = 13).

Survey Point (Catchment ID)	Field Survey Depth (cm)	Method A Simulated Depth (cm)	Method B Simulated Depth (cm)
Point 3 (6799)	90	48.6	0 (Dry)
Point 6 (6310)	70	637.5	0 (Dry)
Point 9 (13106)	30	0 (Dry)	15.0
Point 11 (13106)	300	662.4	0 (Dry)
Point 12 (13106)	300	420.3	0 (Dry)

Point 16 (10247)	85	56.5	0 (Dry)
Point 18 (7278)	180	0 (Dry)	8.5
Point 19 (13106)	60	0 (Dry)	19.7
Point 22 (7498)	60	0 (Dry)	31.2
Point 24 (13106)	200	24.9	0 (Dry)
Point 27 (13106)	80	119.5	3.6
Point 29 (7278)	60	37.5	0 (Dry)
Point 32 (13106)	135	1021.6	18.3
Number of inundated points (n)	-	9	6
Mean Absolute Error (MAE)	-	249.3 cm	74.8 cm
Mean Bias	-	+ 189.8 cm (Overestimation)	- 74.8 cm (Underestimation)

At its nine inundated survey points, Method A produced a mean bias of +189.8 cm and an MAE of 249.3 cm. The error was dominated by strong overestimation at a few points, notably Point 32 (1021.6 cm simulated versus 135 cm observed), Point 11 (662.4 versus 300 cm), and Point 6 (637.5 versus 70 cm), which is consistent with the channel bottleneck depths discussed in Section 3.2; Method A also underestimated the depths at Points 3, 16, 24, and 29. In addition, because the water was injected only at the upstream end of each main river, 23 of the 32 survey points (71.9%) remained dry at the exact-cell level.

In Method B (Rain-on-Grid), only six of the 32 survey points (18.8%) were inundated at the exact cell, while 26 (81.3%) were dry. At these six points, Method B underestimated the surveyed depth at every point, giving a mean bias of −74.8 cm and an MAE of 74.8 cm; five of the six simulated depths are below 20 cm, and Point 18, for example, was simulated at 8.5 cm against 180 cm observed. This underestimation likely reflects the loss of local ponding features (road-side trenches, curbs, and small depressions) through DEM averaging at the 10 × 10 m scale, together with uncertainties in the satellite rainfall and abstraction parameters discussed in Section 4.2.

Recognizing that handheld GPS coordinate uncertainty during field surveys (5–15 meters) and the loss of sub-pixel DEMNAS depressions can shift flood inundation by several cells, the validation of Method B was expanded using a spatial buffer search (neighborhood verification). This analysis was applied to measure the spatial shift tolerance for the 26 points that were dry in their primary cells (Table 5); the same search was not applied to Method A.

Table 5. Distribution of spatial buffer search ranges for Method B across the 26 dry points.

Search Radius Limit	**Number of Points Reached**	**Cumulative Percentage**	**Validation Quality Descriptor**
Radius ≤ 25 meters	6 points	23.1 %	Tolerance identical to GPS error and DEM resolution
Radius ≤ 50 meters	11 points	42.3 %	Shift equivalent to 2 to 5 computational cell sizes (10 m)
Radius ≤ 100 meters	21 points	80.8 %	Acceptable tolerance limit for neighborhood verification
Radius ≤ 150 meters	23 points	88.5 %	Indicates significant topographic offset
Maximum Reach	594.3 meters (Point 8)	100.0 %	Furthest single spatial shift anomaly

Based on Table 5, for 80.8% (21 of 26) of the dry points the rain-on-grid simulation produced an inundated cell of comparable depth within 100 m (overall median distance of 55.8 m); 88.5% were reached within 150 m, while the largest displacement was 594.3 m (Point 8). These distances correspond to roughly 5–10 computational cells and should be read as a spatial tolerance, not as exact-cell agreement.

4. Discussion

4.1. Comparative Implications of Hydrograph Injection vs. Rain-on-Grid

In this study, injecting the lumped synthetic hydrograph at the upstream boundary (Method A) produced results that were less consistent with the field observations than the rain-on-grid approach (Method B) for this multi-catchment event. In the Method A configuration, the full effective runoff volume of each sub-catchment enters through a single upstream cross-section, which is associated with two artifacts: (1) channel bottlenecking, with depths exceeding 15–30 m in the steepest valleys; and (2) a double-lagging effect, in which the hydrograph peak reaches the downstream urban area after the storm window. Both artifacts partly reflect how the Snyder hydrograph was applied here (a catchment-level hydrograph with synthetic, uncalibrated parameters injected at the upstream node) and are not necessarily inherent to hydrograph-based modeling in general; the results should therefore be read as a comparison of these two specific configurations.

The watershed-scale rain-on-grid method (Method B) distributes the water volume across the entire computational mesh from the onset. In this study, this removed the artificial stacking, reducing the area deeper than 5 m from 51.53 km² to 0.39 km², and it reached lateral depressions and tributaries that the single-path configuration did not inundate. At the exact-cell level, however, Method B inundated fewer survey points than Method A (6 versus 9 of 32); its advantage in point coverage appears only when a spatial tolerance is allowed (27 of 32 points within 100 m), which was evaluated for Method B alone. The 0.20 m threshold reduced the wet area of Method B from 192.4 km² to 80.83 km², which shows that the reported footprint is sensitive to this threshold; the threshold was adopted to separate deeper inundation from shallow sheet flow and was not varied in this study.

Compared with earlier studies, Habibi and Nisa (2026) evaluated the same September 2025 event in a single watershed (Tukad Badung) with a binary hit rate, and Pranoto et al. (2026) compared simulated inundation patterns with aerial imagery for a basin in Java. Both used pattern-based agreement measures rather than depth errors at surveyed points. The present study covers 14 sub-catchments and reports depth bias and MAE at 32 surveyed points, but its results cannot be compared directly with hit-rate values, because binary pattern measures can reward overprediction of flood extent (Stephens et al., 2014).

4.2. Uncertainty Factors and Local Depth Validation Limitations

Although the rain-on-grid approach distributed the inundation more plausibly across the floodplain, the exact-point analysis revealed a systematic underestimation of depths (mean bias −74.8 cm). Several factors may contribute to this error, and their individual effects were not separated in this study. First, the topographic averaging effect resulting from resampling the 8.3 m DEMNAS into a 10 m mesh eliminates the model's capacity to represent road trench micro-drainage networks three-dimensionally, causing runoff that should be contained and stacked on the road to disperse into adjacent cells.

Second, the absence of physical hydraulic blocks (weirs) and bridge crossing culverts within the model. Given the vastness of the modeling domain covering 14 sub-catchments with a highly massive

tributary network, inventorying and manually inserting hundreds of cross-river structure geometries into HEC-RAS 2D would demand computationally prohibitive time and data acquisition. Consequently, this simulation utilized a bare-earth channel assumption without structural obstructions. The consequence of this macro-scale assumption's weakness is illustrated near Bendungan Bandung (Point 6). In the field, the dam retained the water flow, resulting in an observed depth of 70 cm; however, the model—without the dam structure in the topography—treated the section as an open bare-earth valley, leading to channel accumulation of 637.5 cm in Method A (while Method B remained dry at this location). Furthermore, literature evidence asserts that the absence of debris blockage calculations at local culverts will cause the model to miss parameters that drastically raise water surface elevations in reality (Fallowfield & Motta, 2024; Franca et al., 2025).

Third, the omission of the subgrid channel method. A one-dimensional (1D) channel flow representation hidden beneath the surface of macro-resolution DEMs can efficiently handle main channel flow transfer (Neal et al., 2012) without requiring the entire computational mesh to be scaled down to 1 meter, which would cause extreme computational burden.

4.3. Practical Implications for Disaster Management in Bali

The dominance of HSG D soil in the HYSOGs250m classification suggests that flood vulnerability in South Bali may be related to soil infiltration characteristics and not only to the capacity of drainage infrastructure. Furthermore, the sensitivity of runoff volume to initial soil moisture (an increase of up to 95%, from 68.6 to 111.2 million m^3, under AMC II, calculated from the abstraction equations without additional hydrodynamic simulation) is a useful warning for BMKG and BPBD. If a comparable storm were to occur on pre-saturated soil (AMC II or AMC III), as may happen during consecutive storms in the rainy season, the runoff volume could be substantially larger and the inundation more extensive.

4.4. Limitations

This study has several limitations. First, rainfall was derived exclusively from satellite products (SITHALA/GPM-IMERG and PERSIANN-CCS) and was not verified against local rain gauges; satellite daily rainfall estimates are uncertain in the complex terrain of Bali, and PERSIANN performed poorly in a gauge-based validation on the island (Rahmawati & Lubczynski, 2018). In this study PERSIANN-CCS was used only to define the storm duration. Second, the effective rainfall depends on the AMC I class, which was assigned from the dry-season criterion and the 5-day antecedent rainfall, and on the 0.05 initial abstraction ratio; because the catchments are ungauged, the resulting runoff volumes could not be calibrated against discharge records. Third, DEMNAS is a surface model that was resampled to a 10 × 10 m mesh; vertical errors on the order of metres have been reported for DEMNAS and other open-source DEMs in Indonesia (Sulistiana et al., 2019; Mutaqin et al., 2023), and channel bathymetry, buildings, and hydraulic structures were not represented. Fourth, the field data consist of 32 discrete points surveyed in July 2026, about ten months after the event, and no independent inundation-extent map was available. Only nine (Method A) and six (Method B) points were inundated at the exact cell, which limits the robustness of the depth-error statistics, and the neighborhood verification was applied to Method B only. Finally, in Method A each sub-catchment hydrograph was injected at the upstream node of the main channel; other ways of applying hydrographs (for example, at the sub-catchment outlet or as lateral inflows) were not tested, so the conclusions apply to the two configurations compared here.

5. Conclusions

This study presents a comparative hydrodynamic evaluation simulating the extreme September 2025 flood event in South Bali. For this satellite-driven, ungauged setting, the results favor the rain-on-grid approach with a sheet-flow noise threshold (0.20 m) over the lumped upstream boundary hydrograph configuration tested here, which produced physical artifacts.

In the hydrograph injection method, 50.6% (51.53 km²) of the inundated area was at depths exceeding 5 m because of upstream channel bottlenecking, the peak time overshot the actual storm window, and 71.9% of the survey points remained dry at the exact-cell level. The rain-on-grid method produced an 80.83 km² inundation footprint, mostly at depths of 0.20–2.00 m, distributed across floodplains and tributaries. At the exact survey cells it inundated six points and underestimated depths (bias −74.8 cm; MAE 74.8 cm); for the 26 points it left dry, 81% had an inundated cell of comparable depth within 100 m (median distance 55.8 m), a neighborhood tolerance that was evaluated for rain-on-grid only.

Nevertheless, the rain-on-grid method still has limited accuracy for local depths (mean bias of −74.8 cm at the six exact-cell points). This is probably related to the lack of geometric representation of micro-scale features (road trenches) and retaining dams, to the 10 m mesh resolution, which cannot represent flow obstruction by debris blockage at bridge piers, and to uncertainty in the satellite rainfall and abstraction parameters, which were not separated in this study. Subgrid channel formulations (Neal et al., 2012) and Height Above the Nearest Drainage (HAND) normalized elevation models (Nobre et al., 2011) are recommended as future developments, together with rain gauge data and independent flood-extent observations for verification, to improve depth accuracy without sacrificing the stability of regional-scale rain-on-grid modeling.

Author Contributions

Conceptualization, G.G.M., R.Y.T., and A.S.; methodology, G.G.M.; software, G.G.M., O.K., and F.T.S.; validation, G.G.M.; formal analysis, G.G.M.; investigation, G.G.M.; resources, G.G.M.; data curation, G.G.M. and J.D.S.; writing—original draft preparation, G.G.M.; writing—review and editing, R.Y.T. and A.S.; visualization, G.G.M. and J.D.S.; supervision, R.Y.T. and A.S.; project administration, G.G.M.; funding acquisition, R.Y.T. All authors have read and agreed to the published version of the manuscript.

Funding

This research was funded by Badan Riset dan Inovasi Nasional (BRIN) through the Riset dan Inovasi untuk Indonesia Maju (RIIM) Wave 10 program No.57186119503.

Data Availability Statement

The spatial datasets (DEMNAS, Sentinel-2, SITHALA, and PERSIANN-CCS) utilized in this study are publicly accessible through their respective official repositories. The HEC-RAS 2D simulation models, Excel calculation spreadsheets, and raw post-disaster field survey records (which contain sensitive residential GPS coordinates) are available from the corresponding author upon reasonable request.

Acknowledgments

The authors express their profound gratitude to the Center of Excellence (CoE) HydroLink for their logistical support during the post-disaster field surveys. We also acknowledge the use of AI assistants

during the data processing and English language editing stages; however, all analyses, scientific interpretations, and final contents remain the sole responsibility of the authors.

Conflicts of Interest

The authors declare no conflict of interest. The funders had no role in the design of the study; in the collection, analyses, or interpretation of data; in the writing of the manuscript; or in the decision to publish the results.

Abbreviations

Abbreviation	Definition
ABM	Alternating Block Method
AMC	Antecedent Moisture Condition
BIG	Badan Informasi Geospasial (Geospatial Information Agency)
BMKG	Badan Meteorologi, Klimatologi, dan Geofisika (Meteorological, Climatological, and Geophysical Agency)
BPBD	Badan Penanggulangan Bencana Daerah (Regional Disaster Management Agency)
BRIN	Badan Riset dan Inovasi Nasional (National Research and Innovation Agency)
CN	Curve Number
DEM	Digital Elevation Model
DEMNAS	Digital Elevation Model Nasional (National DEM of Indonesia)
HAND	Height Above the Nearest Drainage
HEC-RAS	Hydrologic Engineering Center River Analysis System
HSG	Hydrologic Soil Group
MAE	Mean Absolute Error
RIIM	Riset dan Inovasi untuk Indonesia Maju
SCS	Soil Conservation Service

References

Adnyana, I. M., & Wiguna, P. P. K. (2025). Modelling of flood hazard using topographic wetness index in Yeh Ho Watershed, Bali, Indonesia. BIO Web of Conferences, 159, Article 04002. https://doi.org/10.1051/bioconf/202515904002

Badan Informasi Geospasial. (n.d.). DEMNAS: DEM Nasional. https://tanahair.indonesia.go.id/demnas/

Badan Meteorologi, Klimatologi, dan Geofisika. (2024). Data curah hujan dan banjir. BMKG. Accessed from http://www.bmkg.go.id/

Badan Meteorologi, Klimatologi, dan Geofisika. (2025). Prakiraan musim kemarau 2025 di Indonesia. Direktorat Perubahan Iklim, Deputi Bidang Klimatologi, BMKG.

Balai Hidrologi dan Lingkungan Keairan (BHLK), Direktorat Jenderal Sumber Daya Air. (2025). SITHALA: Sistem Informasi Terpadu Hidrologi dan Lingkungan Keairan. https://sithala.bhlk-pu.id/

Bedient, P. B., & Huber, W. C. (1992). Hydrology and floodplain analysis (2nd ed.). Addison-Wesley.

BPBD Provinsi Bali. (2025). Laporan Kejadian Bencana Banjir Provinsi Bali 13 September 2025. Badan Penanggulangan Bencana Daerah Provinsi Bali.

Chow, V. T. (1959). Open-channel hydraulics. McGraw-Hill.

Ebert, E. E. (2008). Fuzzy verification of high-resolution gridded forecasts: a review and proposed framework. Meteorological Applications, 15(1), 51–64. https://doi.org/10.1002/met.25

Fallowfield, L., & Motta, D. (2024). The permanent flood risk of culverts and the impact of increasing debris blockage. Journal of Flood Risk Management, 17(4), e13021. https://doi.org/10.1111/jfr3.13021

Franca, M. J., Cook, R., Pourzangbar, A., Xia, X., Valero, D., Vanzo, D., Bayón, A., & Wright, N. (2025). Why should urban debris dynamics be considered in urban flood management? Water Resources Research, 61(12), e2025WR041574. https://doi.org/10.1029/2025WR041574

Habibi, N. I., & Nisa, A. M. (2026). Analysis of flood inundation distribution based on meteorological factors and land cover using HEC-RAS in the Tukad Badung Watershed (case study: The Bali floods of September 9–10, 2025). GEOGRAPHY: Jurnal Kajian, Penelitian dan Pengembangan Pendidikan, 14(2), 327–343. https://doi.org/10.31764/geography.v14i2.41393

Hawkins, R. H., Jiang, R., Woodward, D. E., Hjelmfelt, A. T., & Van Mullem, J. A. (2002). Runoff curve number method: Examination of the initial abstraction ratio. Proceedings of the Second Federal Interagency Hydrologic Modeling Conference.

Kirpich, Z. P. (1940). Time of concentration of small agricultural watersheds. Civil Engineering, 10(6), 362.

Kusmiyarti, T. B., Wiguna, P. P. K., & Ratna Dewi, N. K. R. (2018). Flood risk analysis in Denpasar City, Bali, Indonesia. IOP Conference Series: Earth and Environmental Science, 123, Article 012012. https://doi.org/10.1088/1755-1315/123/1/012012

Lestari, I., & Herdiansyah, H. (2024). Water Governance: Urban Water Conservation As A Response To Climate Change. International Journal of Conservation Science, 15(1), 627–644. https://doi.org/10.36868/ijcs.2024.01.17

Mutaqin, B. W., Isnain, M. N., Marfai, M. A., & Fatchurohman, H. (2023). Assessing the accuracy of open-source digital elevation models for the geomorphological analysis of very small islands of Indonesia. Applied Geomatics, 15(4), 957–974. https://doi.org/10.1007/s12518-023-00533-8

Neal, J., Schumann, G., & Bates, P. (2012). A subgrid channel model for simulating river hydraulics and floodplain inundation over large and data sparse areas. Water Resources Research, 48(11), W11506. https://doi.org/10.1029/2012WR012514

Nobre, A. D., Cuartas, L. A., Hodnett, M., Rennó, C. D., Rodrigues, G., Silveira, A., Waterloo, M., & Saleska, S. (2011). Height Above the Nearest Drainage – a hydrologically relevant new terrain model. Journal of Hydrology, 404(1–2), 13–29. https://doi.org/10.1016/j.jhydrol.2011.03.051

Prabandari, N. L. P., Pariartha, I. P. G. S., & Tonyes, S. G. (2025). Analisa debit banjir rancangan Bendungan Palasari menggunakan HEC-HMS. PADURAKSA: Jurnal Teknik Sipil Universitas Warmadewa, 14(1), 1–9. https://doi.org/10.22225/pd.14.1.11181.1-9

Pranoto, W. A., Fikri, R. M., Yudianto, D., Rusli, S. R., & Wijaya, O. T. (2026). Quantifying the role of urban development and rainfall shifts in dynamic hydrological extremes. Hydrology, 13(5), Article 123. https://doi.org/10.3390/hydrology13050123

Rahmawati, N., & Lubczynski, M. W. (2018). Validation of satellite daily rainfall estimates in complex terrain of Bali Island, Indonesia. Theoretical and Applied Climatology, 134(1–2), 513–532. https://doi.org/10.1007/s00704-017-2290-7

Ross, C. W., Prihodko, L., Anchang, J., Kumar, S., Ji, W., & Hanan, N. P. (2018). HYSOGs250m, global gridded hydrologic soil groups for curve-number-based runoff modeling. Scientific Data, 5, Article 180091. https://doi.org/10.1038/sdata.2018.91

Setiawan, O. (2012). Analisis variabilitas curah hujan dan suhu di Bali. Jurnal Analisis Kebijakan Kehutanan, 9(1), 66–79.

Snyder, F. F. (1938). Synthetic unit-graphs. Transactions, American Geophysical Union, 19(1), 447–454. https://doi.org/10.1029/TR019i001p00447

Stephens, E., Schumann, G., & Bates, P. (2014). Problems with binary pattern measures for flood model evaluation. Hydrological Processes, 28(18), 4928–4937. https://doi.org/10.1002/hyp.9979

Sulistiana, T., Parapat, A. D., & Aristomo, D. (2019). Analisis akurasi vertikal Digital Elevation Model Nasional (DEMNAS) studi kasus Kota Medan. Prosiding Forum Ilmiah Tahunan Ikatan Surveyor Indonesia (FIT ISI) 2019.

Sutrisnawati, N. K. (2018). Dampak bencana alam bagi sektor pariwisata di Bali. Jurnal Ilmiah Hospitality Management, 9(1), 57–66. https://doi.org/10.22334/jihm.v9i1.144

U.S. Army Corps of Engineers, Hydrologic Engineering Center. (2016). HEC-RAS River Analysis System, Hydraulic Reference Manual, Version 5.0. Davis, CA.